Short communication

Investigation of nano-fibrous selenium and its polypyrrole and graphene composite as cathode material for rechargeable Li-batteries

Dipan Kundu [a,*], Frank Krumeich [b,1], Reinhard Nesper [c,2]

[a] Laboratory of Inorganic Chemistry, Department of Chemistry and Applied Biosciences, ETH Zürich, HCI H130, Wolfgang Pauli Strasse 10, CH-8093 Zürich, Switzerland
[b] Laboratory of Inorganic Chemistry, Dept. of Chemistry and Applied Biosciences, ETH Zürich, HCI H 111, Wolfgang Pauli Strasse 10, 8093 Zürich, Switzerland
[c] Laboratory of Inorganic Chemistry, Department of Chemistry and Applied Biosciences, ETH Zürich, CH-8093 Zürich, Switzerland

HIGHLIGHTS

► Trigonal Selenium nanofibers and t-Se/-polypyrrole, t-Se/-graphene composites were obtained by template free solution route.
► Pure t-Se delivers large specific capacity of 678 Ah kg^{-1} at C/120 current rate.
► Composite formation with polypyrrole minimizes the polarization between charge and discharge voltages.
► Graphene wrapping of the fibers results in a higher specific capacity at moderate current rate.
► Ex-situ XRD confirms conversion reaction of Se with Li.

ABSTRACT

Analogous to the well-known Li–S battery, an electrochemical reaction of two Li + ion with one Se atom ($2Li^+ + Se + 2e^- = Li_2Se$) gives rise to a large specific theoretical capacity of 678 Ah kg^{-1} at around ~2.4 V, resulting in 1627 Wh kg^{-1} of specific energy. Given this much larger energy density than present cathode materials show, selenium nanofiber and its composites with the conducting polymer polypyrrole as well as with graphene have been prepared and electrochemically tested as cathode materials for Li-batteries. At a low current rate of C/120, pure t-Se electrode delivers the theoretical specific capacity, which subsequently drops to 100 Ah kg^{-1} at C/20. As expected, composite formation with polypyrrole and graphene improves the electrochemical performance compared to trigonal selenium (t-Se) fibers. While polypyrrole coating minimizes the polarization between charging and discharging, graphene wrapping enhances the obtainable capacity at moderate cycling rates. Ex-situ X-ray diffraction of the electrode reveals solid solution behavior in the initial stages of lithiation, finally leading to an electrochemical conversion of selenium to Li_2Se.

© 2013 Elsevier B.V. All rights reserved.

1. Introduction

Elemental Sulfur has captivated Li-battery researchers for the last two decades due to the large theoretical specific capacity of 1672 Ah kg^{-1} that it can deliver. It enjoys advantages like high abundance, low cost, and environmental friendliness. However, poor electronic and ionic conductivity of sulfur, and solubility of electrochemical charge–discharge generated polysulfides in the battery electrolyte, endanger the practicality of the lithium sulfur battery [1]. In the Li–S battery, each sulfur atom can react with a maximum of two lithium ions. Selenium being chemically similar to sulfur can be expected to react in a comparable electrochemical manner, which then accounts for a specific capacity of 678 Ah kg^{-1}. Abouimrane et al. have exploited this concept very recently to demonstrate sodium and lithium ion rechargeable batteries based on selenium and selenium–sulfur as cathode [2]. Selenium exhibits a smaller band gap (1.7 eV) compared to sulfur (2.9 eV) [3–5] and thus has a higher intrinsic electronic conductivity which is especially favorable at low operation temperatures. Unlike sulfur, selenium can easily be mold into nanostructures of varying morphology [6–12]. It is well known that higher surface area and thus, better transport kinetics make nanostructured electrode materials superior in several aspects like power density, rate

capability, and cycling stability [13,14]. Nanostructured particles also allow surface modifications which in turn provide better nanophase conductivity and lithium ion diffusion leading to enhanced utilization of electroactive material [14]. In this regard, composite formation with conducting polymers like polypyrrole and nanocarbon like graphene has become an attractive choice in recent times [15–23].

In this work trigonal selenium (t-Se) nanofibers and its composites with polypyrrole and graphene were prepared by simple solution processes and their electrochemical properties for application as cathode material in lithium batteries were systematically evaluated. Ex-situ X-ray diffraction was performed to elucidate the effect of electrochemical lithium insertion on the crystallographic structure of selenium.

2. Experimental procedures

2.1. Synthesis of selenium nanofibers

Sodium selenite (Sigma-Fine Chemicals) was dissolved in distilled water. L-Ascorbic acid (Acros Organics), separately dissolved in water was then added to the above solution at room temperature under magnetic stirring. As ascorbic acid is a 2-electron reducing agent, 2 mol of ascorbic acid is required for 1 mol of Na_2SeO_3. The Na_2SeO_3 solution turned red and then to brick-red after the addition of ascorbic acid. The color change was due to the formation of elemental selenium particles. The reaction was continued for 6 h and finally the product was centrifuged and washed with water and ethanol. The amorphous red selenium was then dispersed in absolute ethanol medium. The dispersion was kept still for about 12 h. The color of the dispersion changed progressively from red to gray suggesting formation of the trigonal selenium (t-Se) from the amorphous phase (α-Se).

2.2. Polypyrrole coating of the Se nanofibers

Chemical oxidative polymerization of pyrrole monomer by ammonium persulfate [24] was utilized to achieve polypyrrole coating of t-Se fibers. Pyrrole monomer (Acros Organics) was dissolved in 20 ml 1 M hydrochloric acid solution. Se nanofibers were then dispersed into this solution under sonication (for 1 h) and cooled to 0 °C. Separately ammonium persulfate (Aldrich-fine Chemicals) (1:1 to Pyrrole monomer) was dissolved in 20 ml 1 M HCl and cooled to 0 °C. This solution was then added at once to the above mixture under magnetic stirring. The reaction was continued for 3 h at 0 °C. The product was centrifuged and then consecutively washed with water, methanol, and acetone.

2.3. Graphene grafting of the Se nanofibers

Graphite oxide dispersion in water was prepared by using natural graphite (AlfaAesar) according to the Brodie method [25]. Graphite oxide dispersion in deionized water was stirred (12 h) and ultrasonicated (1 h) to obtain graphene oxide dispersion in water (1 mg ml^{-1}). Se nanofibers were dispersed in graphene oxide suspension by ultrasonication and the dispersion was hydrothermally treated in a teflon lined steel autoclave at 120 °C–140 °C for 2–3 h. The product was centrifuged, washed with water and ethanol and then dried under vacuum.

2.4. Physical characterization and electrochemical analyzes

X-Ray diffraction (XRD) measurements were carried out using a Bruker D8 diffractometer equipped with Cu-Kα radiation. The overall morphology of the selenium and its composites were studied with field emission scanning electron microscopy (SEM, Zeiss Gemini 1530) and transmission electron microscopy (TEM, Philips CM30ST).

The electrochemical performance of selenium and its composite with polypyrrole and graphene were tested in our home-made stainless steel cells. The working electrode was prepared by mixing active material (75%) with SUPER P nanocarbon (TIMCAL) (15%) and polyvinylidene fluoride (PVDF) (10%) in N-methyl-2-pyrrolidone (NMP). Lithium metal foil served as the counter and as well as the reference electrode. The polypyrrole and graphene amount in the Se/-polypyrrole and Se-/graphene composite was 10 wt% and 6.5 wt%, respectively, which was determined from the weight gain of the t-Se fiber samples after composite formation. The active material content was 67.5% for the Se-/polypyrrole composite electrode and 70.1% for the Se-/graphene composite electrode. The electrode mixture in NMP was sonicated for 1 h to yield a homogenous slurry which was then spread on a coin shaped titanium current collector and dried at 100 °C for 12 h followed by vacuum drying for 6 h. Material loading was about 7–10 mg cm^{-2}. The electrochemical cells were assembled in an argon filled glove box. In general 400 μL of the electrolyte LP 30 which is 1 M LiPF$_6$ in ethylene carbonate (EC) dimethyl carbonate (DMC) (1:1 w/w
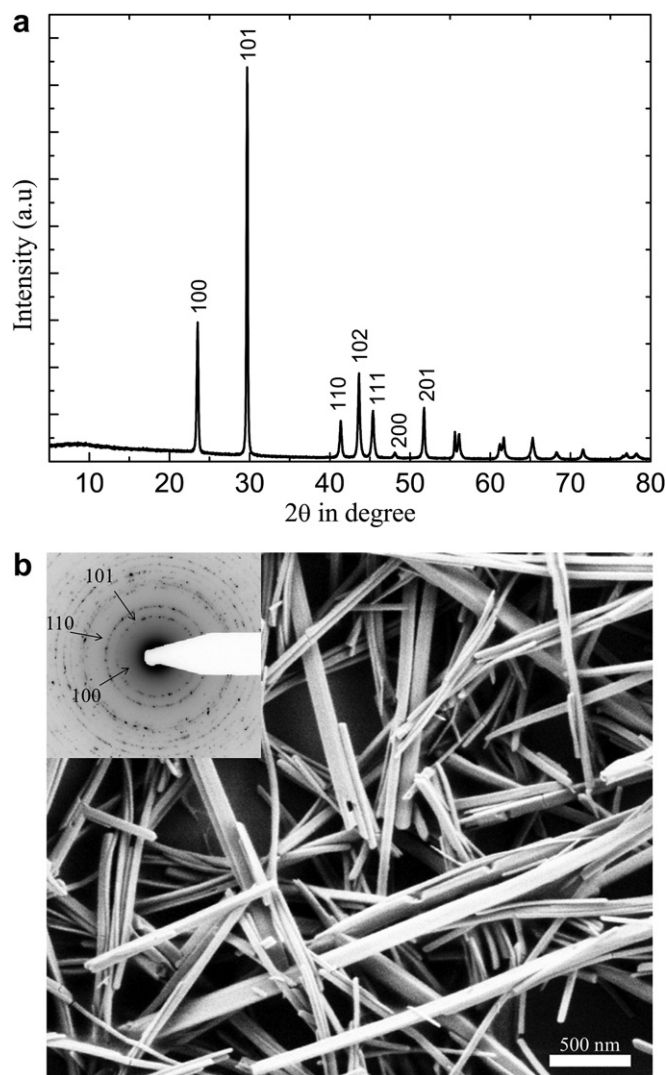

Fig. 1. (a) XRD pattern of the as-synthesized t-Se. (b) A typical SEM image of the t-Se nanofibers with a TEM ED pattern that has been recorded of the fibers, shown in the inset.

provided by MERCK Chemicals, Germany) was used for each test cell. Cyclic voltammetry tests were performed at a scan rate of $100\,\mu V\,s^{-1}$ between 1 and 4 V vs. Li$^+$/Li. Galvanostatic cyclings were performed between 1 and 4 V w.r.t Li$^+$/Li.

For the ex-situ XRD characterization, electrodes were removed from the test cell after electrochemical discharge and put into a small cavity of a plastic sample holder. The cavity, tailor made to accommodate the current collector was then covered with scotch-tape to minimize the exposure to air during analysis. All the manipulations were done in argon atmosphere.

3. Results and discussion

The synthesis method used in this work was followed from an earlier report where ascorbic acid reduction of selenous acid in water under the assistance of β-cyclodextrin was applied to produce selenium nanowires. The presence of β-cyclodextrin was necessary for the formation of t-Se nanowire [26].

$$H_2SeO_3 + 2C_6H_8O_6 \rightarrow Se\downarrow + 2C_6H_8O_6 + 3H_2O$$
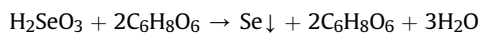
However, we found that the growth of anisotropic t-Se nanostructures can be achieved without the assistance of any templating agent; as for simple kinetic reasons t-Se grows anisotropically along the [001] chain direction. When aged in ethanol, α-Se molecules (Se$_8$) dissolve slowly to generate more reactive selenium atoms which induce recrystallization toward t-Se chains. The t-Se seeds grow anisotropically to form the t-Se nanorods. Utilization of surfactant free active material is crucial for battery electrode application as the insulating organic impurities not only contribute to the

inactive mass but also lower the overall electronic and eventually ionic conductivity of the electrode mixture. In this regard Se fibers synthesized by our surfactant free process is more suitable for electrode fabrication.

The amorphous nature of the brick red color selenium obtained by the ascorbic acid reduction of sodium selenite was confirmed by XRD (Fig. S1a). Fig. 1a shows the XRD pattern of the product obtained by ethanol aging of α-Se. All the diffraction peaks could be indexed as those of the trigonal phase of selenium (t-Se). The chemical purity of the t-Se in the polypyrrole and graphene composite samples was examined by XRD (Fig. S2). The identical diffraction patterns to that of the pristine t-Se affirm that t-Se is unaltered in the composites. The SEM investigation revealed branched network morphology for α-Se (Fig. S1b). Whereas, a fiber like morphology (Fig. 1b) was observed for the as-synthesized t-Se under SEM. The nanofibers are several micrometers in length and the diameters vary from 50 to 200 nm. The concentric rings in the TEM ED pattern (inset: Fig. 1b) recorded of the fibers correspond to lattice planes of the trigonal selenium. The morphology and structural features of the composites was investigated by SEM and TEM. The roughness and spots on the Se fiber's surface as seen in the SEM image (Fig. 2a) of the Se/-polypyrrole composite can directly be correlated to 8–12 nm thick polypyrrole coating clearly visible in its representative TEM image (Fig. 2c). It is apparent that the controlled oxidative polymerization of pyrrole monomers results in a thin homogenous layer of polypyrrole coating on the Se nanofibers. The graphene wrapping of the Se fibers is clearly demonstrated in both the SEM (Fig. 2b) and TEM (Fig. 2d) image of the Se/-graphene composite. It is evident that the graphene sheets, which deposit and wrap around the t-Se fibers are composed of
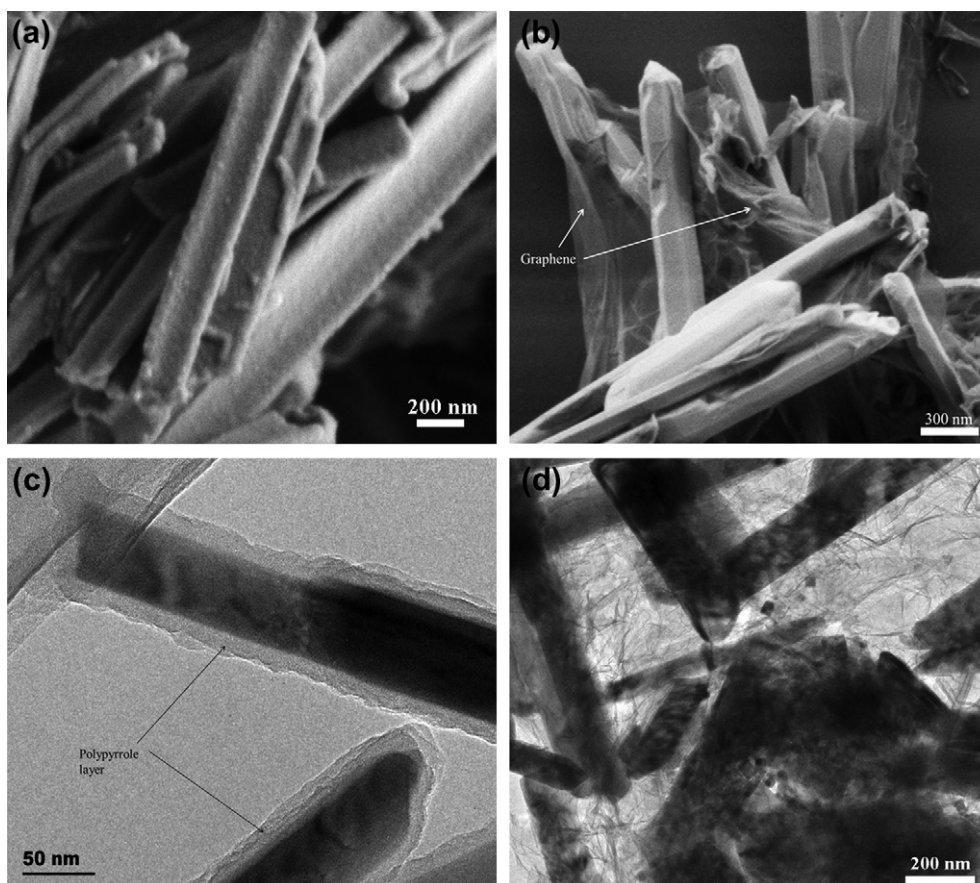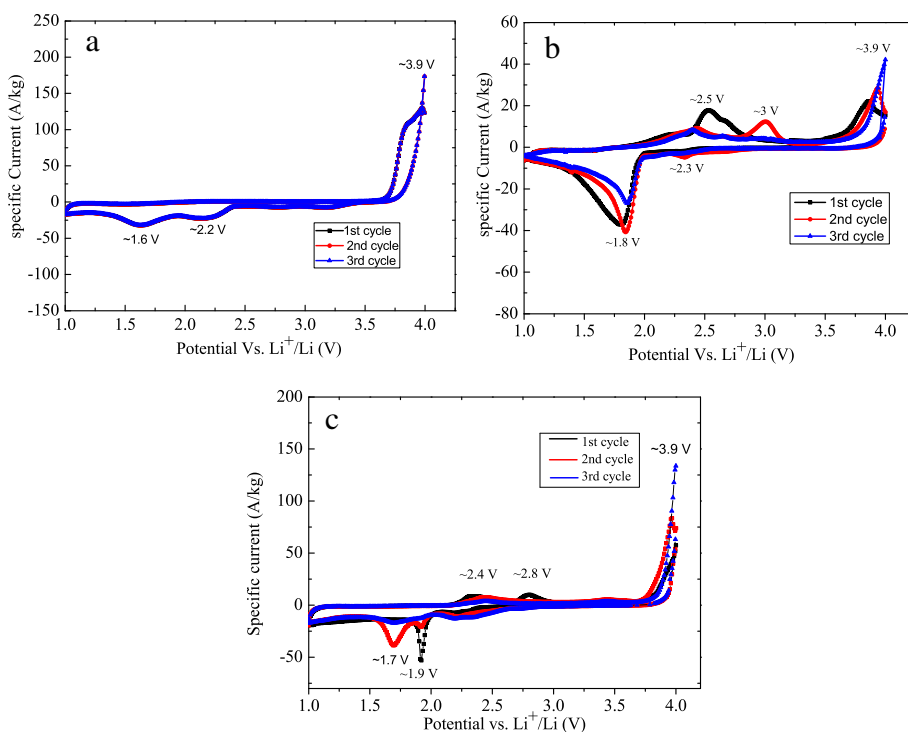

Fig. 2. (a) SEM and (c) TEM image of polypyrrole coated Se fibers. (b) SEM and (d) TEM image of graphene wrapped Se fibers.

Fig. 3. Cyclovoltammetric behavior of (a) pristine t-Se, (b) Se/-polypyrrole, and (c) Se/-graphene electrode performed at a scan rate of 0.1 mV s^{-1} between 1 and 4 V against Li^{+}/Li.

several monolayers of graphene. Hydrothermal treatment of graphene oxide promoted the dehydration mediated formation of graphene.

The cyclovoltammograms (CV) of t-Se fibers, Se/-polypyrrole, and Se/-graphene composites are presented in Fig. 3. The CV

curves demonstrate reversible insertion and de-insertion of lithium ions into/from the selenium fibers. For all of the three electroactive samples multiple reduction peaks appear in the window of 3–1.5 V. However, the number of reduction peaks and their onset voltage differ from each other. Only one oxidation peak appears for pure t-
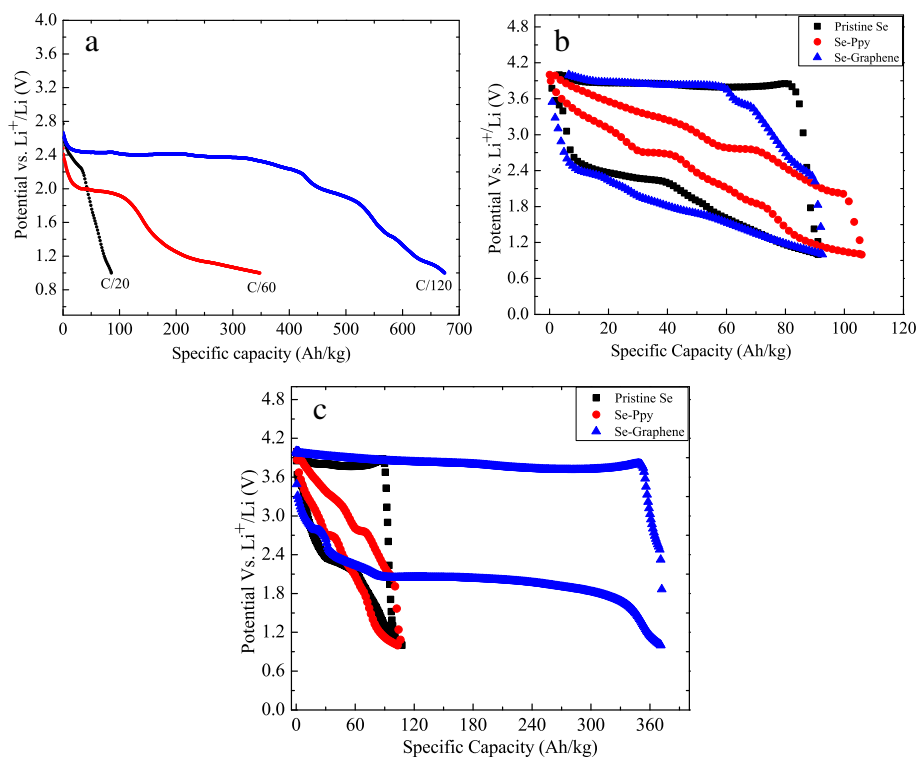
Fig. 4. (a) Galvanostatic discharge curves of pristine t-Se electrode at different current rate; (b) and (c) charge/discharge curves of pristine t-Se, Se-/polypyrrole, and Se/-graphene electrode in the 1st, and 6th galvanostatic cycle, respectively.

Se at around ∼3.9 V in the charging process. Whereas for the polypyrrole and graphene composite, multiple oxidation peaks appear in the charging reaction along with a sharp peak at ∼3.9 V, clearly indicating the activation of new electrochemical processes due to the composite formation. However, with repeated cycling ∼3.9 V oxidation peak becomes stronger and the other oxidation peaks fade out and the CV curves of the polypyrrole and graphene composite electrodes start resembling the CV of the pure t-Se electrode.

Fig. 4a is typical discharge characteristics of pure t-Se at different current rates. The theoretical specific capacity is achieved at a very low current rate of C/120 (where 1 C rate corresponds to insertion/extraction of 2 lithium ions per Se atom in 1 h at an equivalent capacity of 678 Ah kg^{-1}). At this rate more than 400 Ah kg^{-1} of specific capacity is obtained in the plateau region around 2.5 V. At an increased current rate of C/60, achievable capacity drops to half of the theoretical value and the plateau region around 2.5 V becomes small. Fig. 4b, and c compare the charge–discharge characteristics of the pristine t-Se, Se/-polypyrrole, and Se/-graphene electrodes in the 1st and 6th galvanostatic cycle, respectively, performed at a current rate of C/13 (50 A kg^{-1}). Pure t-Se and Se/-graphene electrode delivers a reversible capacity of 90 Ah kg^{-1} in the first cycle. The corresponding discharge profiles of these two electrodes look rather similar with a plateau like region at around ∼2–2.4 V, which is possibly related to the polyselenide formation (similar to the polysulfide formation during discharge of the sulfur electrode in Li–S battery setup) followed by a sloping part. The charge curve has a nearly flat plateau at around 3.9 V. For the Se/-polypyrrole composite, both the discharge and charge curves are relatively sloping in nature and consist of multiple small plateaus. Clearly the Se/-polypyrrole electrode has less polarization between discharge and charge voltages in comparison to both pure t-Se and Se/-graphene electrode, suggesting faster electrochemical reaction kinetics for the polypyrrole composite electrode. Both the pristine t-Se and graphene composite electrode demonstrate capacity increment with cycling. While capacity of the t-Se electrode increases to 110 Ah kg^{-1} in the 6th cycle, graphene composite electrode shows a dramatic increase in capacity to 375 Ah kg^{-1} in as many cycles. Interestingly, the plateau region at around ∼2 V, which is most likely related to the phase transformation of selenium to polyselenides, contributes largely to the increased capacity of graphene composite electrode. However, this large capacity value obtained for graphene composite electrode is not sustainable and drops quickly to 125 Ah kg^{-1} within 15 cycles (Fig. S3). It should be noted that graphene composite formation is able to engage most of the Se fibers in the electrochemical process leading to a high specific capacity. The rapid capacity drop can be attributed to the large volume change and particle disintegration leading to the pulverization of the electrode, and consequent electrical contact loss between active material and the current collector. Fig. S4 demonstrates the corresponding electrochemical cycleability of t-Se, Se/-polypyrrole, and Se/-graphene electrodes. Notably, the specific capacity of pristine t-Se electrode slowly increases with cycling possibly due to particle disintegration and participation of more active particles in the electrochemical process. For the Se/-polypyrrole composite electrode, the specific capacity value decreases slowly reaching 60 Ah kg^{-1} in the 50th cycle.

The pristine t-Se electrode was examined by ex-situ XRD to elucidate any structural change induced by the electrochemical lithium insertion. As applied current density had large influence on the obtainable discharge capacity and hence the lithiation level, the pristine t-Se electrode was discharged at two different current rates to perform XRD investigation. Ex-situ X-ray diffraction of the electrode (Fig. 5a), which was discharged at a rate of C/100, reveals almost complete collapse of the trigonal structure of selenium. At

this slow discharge rate a discharge capacity (660 Ah kg^{-1}) close to the theoretical value was obtained confirming a near complete reaction of selenium with lithium. All of the t-Se diffraction peaks almost disappear after the 1st electrochemical discharge reaction indicating a complete disintegration of the trigonal structure of t-Se. As the XRD was performed with the electrode mix on the titanium current collector, the peaks due to Ti remain unchanged after the discharge reaction and serve as reference. The new peaks that appear after the discharge can be due to electrolyte decomposition or more likely from the new species formed during discharge. None of the peaks match with Li$_2$Se, the expected end product of the electrochemical reaction of selenium and lithium. However, absence of Li$_2$Se peaks is most likely due its amorphous nature. Fig. 5b depicts the XRD patterns of the electrode mixture before and after electrochemical discharge that was carried out at a rate of C/20 (∼33 A kg^{-1}). Although all the diffraction peaks corresponding to t-Se could still be visible, intensity of the peaks diminish after the discharge reaction. At this current rate, only ∼0.35 Li$^+$ per
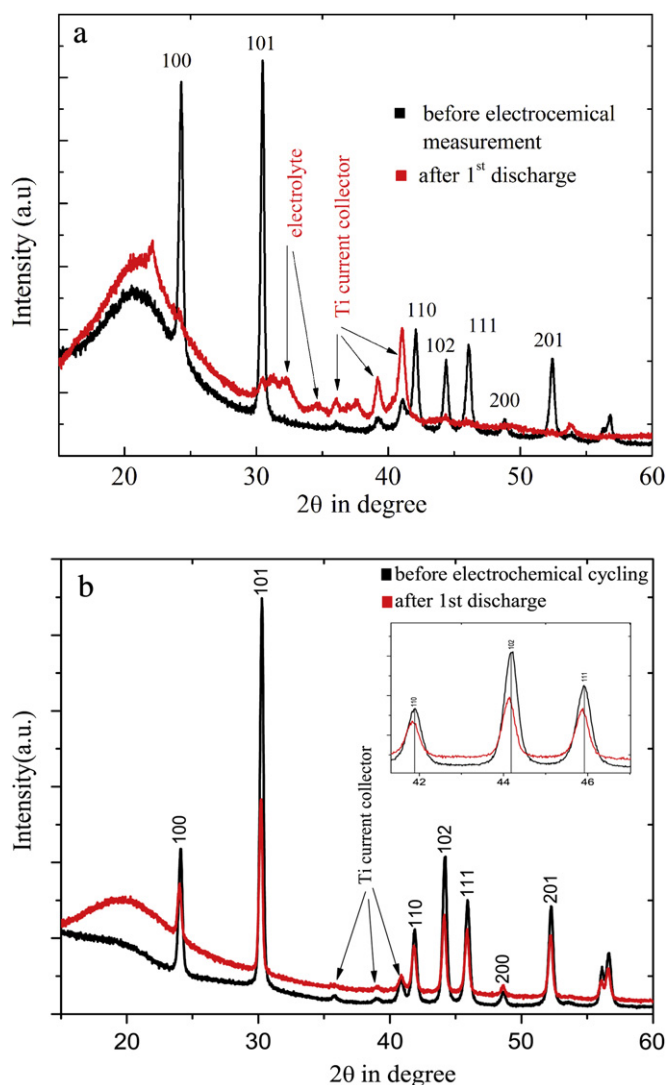

Fig. 5. Ex-situ XRD patterns of the electrode before and after electrochemical discharge in a half cell against Li anode (a) at C/100 rate, and (b) at C/20 rate. Inset in (b) shows shift in the peak positions of the t-Se after electrochemical discharge. In both the case XRD was performed with the material on the titanium current collector and hence the Ti metal peaks are visible in both before and after the discharge and serve as reference.

selenium atom are reacted; obviously such a low lithiation level does not destroy the trigonal structure of selenium.

At a closer look (inset: Fig. 5b), a very small shift in the peak positions to lower 2θ values is observed, which indicates to an increase in the unit cell volume as expected due to lithium insertion. From this study we can infer that the electrochemical lithium insertion of t-Se proceeds in a solid solution pathway during the beginning of discharge reaction, and leads to a complete structural disintegration at the end of complete lithiation.

4. Conclusions

Selenium nanofibers and its polypyrrole and graphene composites were synthesized by surfactant free solution processes. These materials were tested electrochemically in lithium test cells to evaluate the feasibility of a Li–Se battery similar to the Li–S system. Pure t-Se fibers exhibit a large discharge capacity of 678 Ah kg^{-1} at a current rate of C/120. Composite formation with the conducting polymer polypyrrole and with graphene nano sheets proves to be beneficial for electrochemical performance. The large voltage hysteresis of the pure t-Se electrode considerably disappears for t-Se/-polypyrrole composite. Graphene composite formation engages a maximum amount of t-Se fibers in the electrochemical process resulting in a specific capacity of $\sim$375 Ah kg^{-1} even at a rate of C/13, hinting toward a better kinetics for the graphene composite electrode. Ex-situ X-ray diffraction of a pure t-Se electrode, discharged at a very slow rate, reveals complete collapse of the trigonal structure of selenium, as expected from the assumption of complete conversion of Se to Li$_2$Se at the end of discharge. Overall, the present study reveals that even though the basic electrochemical reaction of Li and Se is similar to that of Li and S, the underlying electrochemical processes might be quite different from each other. Trigonal selenium seems promising as a prospective cathode material for Li-battery applications due to its high specific capacity and it's easy processing as nanomaterials and into composites. Use of much finer nanoparticles ($<$20–50 nm) and a superior conductive composite formation that can withstand the large volume change upon lithium exchange possibly holds the key to a successful application.

Acknowledgments

Appendix A. Supplementary data

Supplementary data related to this article can be found at http://dx.doi.org/10.1016/j.jpowsour.2013.02.050.

References

[1] J. Xiulei, L.F. Nazar, Journal of Materials Chemistry 20 (2010) 9821–9826.
[2] A. Abouimrane, D. Dambournet, K.W. Chapman, P.J. Chupas, W. Weng, K. Amine, Journal of the American Chemical Society 134 (2012) 4505–4508.
[3] S. Itoh, K. Nakao, Journal of Physics C-Solid State Physics 17 (1984) 3373–3389.
[4] A.K. Abass, N.H. Ahmad, Journal of Physics and Chemistry of Solids 47 (1986) 143–145.
[5] M. Springborg, R.O. Jones, Journal of Chemical Physics 88 (1988) 2652–2658.
[6] G.S. Cao, X. Juan Zhang, L. Su, Y. Yang Ruan, Journal of Experimental Nano-science 6 (2011) 121–126.
[7] J. Ma, C. Sun, J. Lian, W. Zheng, Crystal Research and Technology 44 (2009) 391–394.
[8] C. An, K. Tang, X. Liu, Y. Qian, European Journal of Inorganic Chemistry 2003 (2003) 3250–3255.
[9] Y. Ma, L. Qi, J. Ma, H. Cheng, Advanced Materials 16 (2004) 1023–1026.
[10] U.K. Gautam, M. Nath, C.N.R. Rao, Journal of Materials Chemistry 13 (2003) 2845–2847.
[11] H. Zhang, D. Yang, Y. Ji, X. Ma, J. Xu, D. Que, The Journal of Physical Chemistry B 108 (2004) 1179–1182.
[12] X. Gao, T. Gao, L. Zhang, Journal of Materials Chemistry 13 (2003) 6–8.
[13] J.B. Goodenough, Y. Kim, Chemistry of Materials 22 (2010) 587–603.
[14] P.G. Bruce, B. Scrosati, J.-M. Tarascon, Angewandte Chemie International Edition 47 (2008) 2930–2946.
[15] O. Mao, R.L. Turner, I.A. Courtney, B.D. Fredericksen, M.I. Buckett, L.J. Krause, J.R. Dahn, Electrochemical and Solid State Letters 2 (1999) 3–5.
[16] Y.J. Mai, X.L. Wang, J.Y. Xiang, Y.Q. Qiao, D. Zhang, C.D. Gu, J.P. Tu, Electrochimica Acta 56 (2011) 2306–2311.
[17] S. Stankovich, D.A. Dikin, G.H.B. Dommett, K.M. Kohlhaas, E.J. Zimney, E.A. Stach, R.D. Piner, S.T. Nguyen, R.S. Ruoff, Nature 442 (2006) 282–286.
[18] H. Wang, L.-F. Cui, Y. Yang, H. Sanchez Casalongue, J.T. Robinson, Y. Liang, Y. Cui, H. Dai, Journal of the American Chemical Society 132 (2010) 13978–13980.
[19] N. Li, M. Zheng, H. Lu, Z. Hu, C. Shen, X. Chang, G. Ji, J. Cao, Y. Shi, Chemical Communications 48 (2012) 4106–4108.
[20] X. Liang, Y. Liu, Z.Y. Wen, L.Z. Huang, X.Y. Wang, H. Zhang, Journal of Power Sources 196 (2011) 6951–6955.
[21] Y. Kim, Q.T. Ta, H.C. Dinh, P.K. Aum, I.H. Yeo, W. Il Cho, S.I. Mho, Journal of The Electrochemical Society 158 (2011) A133–A138.
[22] F.H. Tian, L. Liu, Z.H. Yang, X.Y. Wang, Q.Q. Chen, Materials Chemistry and Physics 127 (2011) 151–155.
[23] C. Lifeng, S. Jian, C. Fangyi, T. Zhanliang, C. Jun, Journal of Power Sources 196 (2011) 2195–2201.
[24] S.P.M. Chougule, P. Godse, R. Mulik, S. Sen, V. Patil, Soft Nanoscience Letters 1 (2011) 6–10.
[25] B.C. Brodie, Philosophical Transactions of the Royal Society of London 149 (1859) 249–259.
[26] Q. Li, V.W.-W. Yam, Chemical Communications (2006) 1006–1008.